Diffusion-Limited Reactions in Nanoscale Electronics *

Ryan M. Evans † Arvind Balijepalli ‡ Anthony J. Kearsley†

September 22, 2020

Abstract

To quantify interactions between drug molecules and target receptors, a novel nanoscale electronics instrument is under development. The instrument consists of two regions: a biological region, and an electronics region. The biological region consists of a well containing a buffer fluid, and receptors immobilized on a biochemical gate at the well-surface. The electronics regions consists of a semiconductor channel, through which current is flowing from source to drain. During a typical experiment ligand molecules are injected at the top of the well, and diffuse to the surface to bind with receptors. Ligand binding with receptors modulates current flow through the semiconductor channel, thereby producing a time-dependent current signal which can be used to study the biochemical process of interest. To quantify the coupling between diffusion and reaction, a partial differential equation model for this system is developed. It is shown that one can exploit disparate length scales associated with the device to reduce the coupled PDE model to a single nonlinear integrodifferential equation for the reacting species concentration. A numerical solution to this equation is found with the method of lines, and results reveal the presence of a depletion region on the biochemical gate. The size of the depletion region is directly related to the Damköhler number.

1 Introduction

Recent advances in genetics and medical technology have put physicians and researchers closer to realizing preciesion medicine–an approach which centers on tailoring treatment protocols to individuals based upon their environment, genetic information, and lifestyle. To customize treatment protocols physicians must be able to quickly measure markers and evaluate the efficacy of a given therapy, which requires precise measurements of drug molecule-protein interactions. Although technology such as Surface

*Submitted to the editors October 18, 2017.

†Applied and Computational Mathematics Division, National Institute of Standards and Technology, Gaithersburg, MD 20899, USA. (ryan.evans@nist.gov, anthony.kearsley@nist.gov) **Funding:** The first author was supported by the National Research Council through a postdoctoral fellowship.

‡Engineering Physics Division, National Institute of Standards and Technology, Gaithersburg, MD 20899, USA. (arvind.balijepalli@nist.gov)

Plasmon Resonance (SPR) biosensing, mass spectroscopy, or Nuclear Magnetic Resonance (NMR) spectroscopy can be used, these tools are time-consuming, expensive, and cannot be utilized point-of-care. This has motivated the development of a novel nanoscale electronics instrument at NIST, designed to provide fast, accurate, inexpensive, and portable measurements of interactions between drug molecules and their target receptors. A schematic of the device is depicted in Figure 1.1. The instrument is partitioned into two regions: a biological region and an electronics region. The electronics region consists of a semiconductor channel through which current flows from source to drain. The biological region consists of a well containing a buffer fluid, and receptors immobilized on a biochemical gate at the well floor. During a typical experiment ligand molecules are injected at the top of the well at concentration $C(x,y,t)$, and diffuse to the surface to bind with receptors confined to the biochemical gate, creating bound ligand molecules at concentration $B(x,t)$. Ligand binding with receptors on the biochemical gate modulates current flow through the semiconductor channel, resulting a time-dependent current signal which may be used measure drug molecule-protein interactions. For example, the signal thus obtained could be used to estimate kinetic rate constants associated with these reactions.

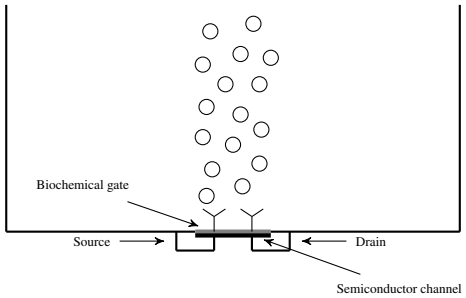

Figure 1.1: Schematic of the nanoscale electronics instrument. Ligand molecules injected at the top of the well diffuse to the surface to bind with receptors immobilized on the biochemical gate. This schematic is not drawn to scale. In particular, the length of the well floor is on the order of millimeters, while the length of the biochemical gate is on the order of micrometers.

This instrument is an example of a Biological Field Effect Transistor (Bio-FET), and has a number of advantages. In contrast with techniques such as fluorescent microscopy, this instrument does not require protein labeling. Such techniques are not only economically disadvantageous, but also introduce the possibility of modifying protein activity, rendering any measurements suspect. Furthermore, this instrument enjoys high sensitivity and selectivity. In addition, the instrument is designed to be portable and inexpensive.

Since the ability to interpret experimental results relies on an accurate mathematical model, this nanoscale electronics instrument raises several interesting mathematical questions. Of particular interest is a quantitative description of the coupling between bound ligand evolution and diffusion. To the authors' knowledge this is a previously unexplored area of mathematical inquiry, though a Poisson-Boltzman approach

to model sensor physics is common. For example in [4] Heitzinger *et al*. use the Poisson-Boltzman equation to develop a multiple-scale model for the electric potential distribution within semiconductors of planar and nanowire field effect biosensors. Therein, the authors model these devices using three layers: a semiconductor layer, a dielectric layer, and a discrete layer of biomolecules immobilized on the dieletric layer. Homogenization techniques are employed to reconcile the biomolecule length scale with the semiconductor length scale, and interface conditions for the biomolecule-dielectric interface are derived. It must be noted that there are several important differences between [4] and the present manuscript. Perhaps the most stark contrast is that [4] focuses on the electric potential distribution within the semiconductor channel, whereas the present manuscript concerns the coupling between reaction and diffusion. Furthermore, while the authors of [4] model the biomolecule layer with a discrete number of biomolecules and use homogenization techniques, in the present manuscript we adopt a continuum perspective. Moreover, [4] assumes a *steady* distribution of biomolecules on the dielectric layer, while the present manuscript concerns the *evolution* of $B(x,t)$. This is an experimentally relevant difference: the instrument under consideration produces time-dependent data and an unsteady model for $B(x,t)$ is necessary. For example, with a steady model one could estimate the equilibrium dissociation rate constant in a given reaction, however it is not clear how one could a steady model to extract the kinetic rate constants themselves.

A Poisson-Boltzman approach is also employed in [5], where a one-dimensional Poisson-Boltzman equation is used to model a layer of biological macromolecules on the gate of a metal-oxide-semiconductor transistor. A similar one-dimensional Poisson-Boltzman model is also described in [1]. A three-dimensional model is proposed in [2], where the authors model the electric potential in an aqueous solution and semiconductor channel with a Poisson-Boltzman equation. These two regions are coupled through interface conditions derived from Monte-Carlo simulations which calculate the charge distribution resulting from a layer of charged biomolecules on the semiconductor's surface. For other examples of a Poisson-Boltzman approach one may see [3, 6, 8]. Note that all of these models assume a steady distribution of biomolecules, and thus cannot be used to analyze time-dependent data.

In [7] Hietzinger and coworkers calculate numerical values for the kinetic parameters governing adsorption and desorption processes of carbon monoxide at a tin dioxide single-nanowire gas sensor. Therein, the authors adopt a continuum perspective by modeling surface reactions on a single-nanowire gas sensor through a set of differential equations. However, in [7] the authors simply apply the well-stirred kinetics approximation in which gaseous carbon monoxide transport is completely divorced from adsorption and desorption processes at the surface. This reduces their model to a nonlinear set of Ordinary Differential Equations, which can be used to estimate kinetic rate constants involved in the reaction of interest.

Hence, although the significance of the interplay between reaction and diffusion in biosensors is well-known, to date these effects have not been quantified in the context of Bio-FETs. In the present manuscript we develop a quantitative description of the coupling between reaction and diffusion for the novel nanoscale electronics instrument described herein. In particular, we consider the experimentally relevant limit of very low ligand concentrations–*i.e.*, on the order of pico- to femtomolar concentrations–and

very fast assocation rates. This problem is interesting because it involves multiple time and length scales. While the length scale of the well is on the order of millimeters, the length scale of the biochemical gate is on the order of micrometers. Furthermore, while the rate at which ligand molecules diffuse through the well is very slow, the rate at which they bind with receptors is very fast. The consideration of multiple time and length scales reveals that the evolution of the reacting species concentration $B(x,t)$ depends heavily upon a diffusive boundary layer near the surface.

We begin in Section 2 by developing a mathematical model for an experiment in which ligand molecules are continuously and uniformly injected into the nanoscale electronics instrument. It must be noted that although, in practice experimentalists inject ligand molecules over only a very narrow portion of the well, this idealization was made to obtain useful analytic results. Future work will include a comparison of experimental data with the present model. Given this assumption, our model takes the form of a diffusion equation coupled to a Partial Differential Equation (PDE) describing reaction on the biochemical gate. In Subsection 2.1 the governing equations are presented, and it is shown that there are multiple time and length scales associated with the experiment. In Subsection 2.2, techniques from complex analysis are used to reduce the coupled PDE system to a single nonlinear Integrodifferential Equation (IDE) for the reacting species concentration. A quadrature-free numerical solution based on the method of lines is developed in Section 3, where it is shown that this method acheives first-order accuracy despite a singular convolution kernal. Results and their physical interpretations are discussed in Section 4, and concluding remarks are given in Section 5.

2 Governing Equations

2.1 Mathematical Model

We consider the geometry shown in Figure 1.1, and take our domain to be the rectangle $(\widetilde{x},\widetilde{y}) \in [0,\widetilde{L}] \times [0,\widetilde{H}]$, with the origin $(0,0)$ located at the lower-left corner of the well. The parameters $\widetilde{L}$ and $\widetilde{H}$ are the height and length of the well respectively; for parameter values see Table 2.1. Throughout manuscript paper tildes are used to denote dimensional quantities. Receptors are confined to the biochemical gate on the sensor surface, which occupies the very narrow region $(\widetilde{x},\widetilde{y}) \in [-\widetilde{l}_{\rm s}/2+\widetilde{L}/2,\ \widetilde{L}/2+\widetilde{l}_{\rm s}] \times 0 = [\widetilde{x}_{\rm min},\widetilde{x}_{\rm max}] \times 0$, where $\widetilde{l}_{\rm s}$ denotes length of the biochemical gate and $[\widetilde{x}_{\rm min},\widetilde{x}_{\rm max}] := [-\widetilde{l}_{\rm s}/2+\widetilde{L}/2,\ \widetilde{L}/2+\widetilde{l}_{\rm s}]$. It is important to note the while the length scale of the well is on the order of millimeters, the length scale of the biochemical gate is on the order of micrometers.

Assuming that ligand molecules are continuously and uniformly injected at the top of the well, ligand transport is governed by the diffusion equation which is expressed

Table 2.1: Bounds for dimensional and dimensionless parameters are given below.

Necessary Parameters			Ancillary Parameters	
Parameter	Range	Reference	Parameter	Range
$\widetilde{D}$ (cm^2/s)	10^{-6}		D_w	4×10^{-3}–40
$\widetilde{k}_\mathrm{a}$ ($\mathrm{cm}^3\cdot(\mathrm{mol}\cdot\mathrm{s})^{-1}$)	10^{11}–10^{12}		D	4×10^{3}–4×10^{7}
$\widetilde{k}_\mathrm{d}$ (s^{-1})	10^{-5} – 1		Da_w	3321.1–66420.0
$\widetilde{C}_\mathrm{u}$ ($\mathrm{mol}\cdot\mathrm{cm}^{-3}$)	10^{-18}–10^{-15}		Da	3.32110–66.4200
$\widetilde{R}_\mathrm{t}$ ($\mathrm{mol}\cdot\mathrm{cm}^{-2}$)	6.6422×10^{-14}–1.3284×10^{-13}		K	10^{-2}–10^{7}
$\widetilde{H}$ (cm)	0.2		ε	.4
$\widetilde{L}$ (cm)	0.5		l_s	10^{-3}
$\widetilde{l}_s$ (cm)	5×10^{-4}			

in dimensionless form as:

$$\frac{\partial C}{\partial t} = D_\mathrm{w}\left(\varepsilon^2\frac{\partial^2 C}{\partial \bar{x}^2}+\frac{\partial^2 C}{\partial \bar{y}^2}\right), \tag{2.1a}$$

$$C(\bar{x},\bar{y},0)=0, \tag{2.1b}$$

$$\frac{\partial C}{\partial \bar{x}}(0,\bar{y},t)=\frac{\partial C}{\partial \bar{x}}(1,\bar{y},t)=0. \tag{2.1c}$$

Equation (2.1a) is the diffusion equation, (2.1b) is the initial condition, and (2.1c) are no-flux conditions which hold on the sides of the well. In writing (2.1a)–(2.1c), we have nondimensionalized the spatial variables $\widetilde{x}$ and $\widetilde{y}$ using the well dimensions by setting $\bar{x}=\widetilde{x}/\widetilde{L}$ and $\bar{y}=\widetilde{y}/\widetilde{H}$. Additionally, since we are interested in reaction dynamics on the sensor surface, the time variable has been scaled by the forward reaction rate $t=\widetilde{k}_\mathrm{a}\widetilde{C}_\mathrm{u}\widetilde{t}$. Here $\widetilde{C}_\mathrm{u}$ is the uniform injection concentration at the top of the well.

In (2.1a)–(2.1c) $\varepsilon=O(1)$ is the aspect ratio, and

$$D_\mathrm{w}=\frac{\widetilde{D}}{\widetilde{H}^2\widetilde{k}_\mathrm{a}\widetilde{C}_\mathrm{u}}=\frac{\widetilde{D}/\widetilde{H}^2}{\widetilde{k}_\mathrm{a}\widetilde{C}_\mathrm{u}} \tag{2.2}$$

is the dimensionless diffusion coefficient, which is the ratio of the time scale on which ligand molecules diffuse through the well $\widetilde{D}/\widetilde{H}^2$ to the time scale for forward reaction $\widetilde{k}_\mathrm{a}\widetilde{C}_\mathrm{u}$. The subscript w indicates that the independent variables are currently scaled with the well dimensions. It is seen in Table 2.1 that $D_\mathrm{w}=O(10^{-3})$–$O(10)$, which implies that diffusion through the well is either slower or slightly faster than the forward reaction rate. The latter case is interesting since it implies that the time scale diffusion through the well is slightly *faster* than the time scale of forward reaction; this phenomenon arises in the limit of femtomolar ligand concentrations $\widetilde{C}_\mathrm{u}$.

To state the bottom boundary condition associated with (2.1a)–(2.1c) we observe that when $(\bar{x},\bar{y})\notin[\bar{x}_\mathrm{min},\bar{x}_\mathrm{max}]\times0$ there is no flux through the surface of the well, while when $(\bar{x},\bar{y})\in[\bar{x}_\mathrm{min},\bar{x}_\mathrm{max}]\times0$ the diffusive flux normal to the binding surface is used in forming bound ligand $B(\bar{x},t)$. These two conditions are expressed compactly as:

$$(\mathbf{n}\cdot\nabla C)|_{y=0}=\mathrm{Da}_\mathrm{w}\,\chi_\mathrm{s}\,[-(1-\widetilde{B})\widetilde{C}(x,0,t)+KB]. \tag{2.3}$$

In (2.3) $\mathbf{n} = (0,-1)$ denotes the outward unit normal vector, χ_s is the characteristic function defined as

$$\chi_s(\bar{x}) = \begin{cases} 1 & \bar{x} \in [\bar{x}_{\min}, \bar{x}_{\max}], \\ 0 & \bar{x} \notin [\bar{x}_{\min}, \bar{x}_{\max}], \end{cases} \tag{2.4}$$

and $K = \widetilde{k}_d/(\widetilde{k}_a\widetilde{C}_u)$ is the dimensionless equilibrium dissociation rate constant. Furthermore, since the bound ligand concentration is governed by the kinetics equation

$$\frac{\partial B}{\partial t} = (1-B)C(x,0,t) - KB, \tag{2.5a}$$

$$B(x,0) = 0, \tag{2.5b}$$

we can express (2.3) as

$$\frac{\partial C}{\partial y}(x,0,t) = \mathrm{Da_w}\frac{\partial B}{\partial t}. \tag{2.6}$$

The complete Partial Differential Equation (PDE) system is then given by (2.1), (2.5), and (2.6).

In (2.3) and (2.6), the important dimensionless parameter

$$\mathrm{Da_w} = \frac{\widetilde{H}\widetilde{k}_a\widetilde{R}_t}{\widetilde{D}} = \frac{\widetilde{k}_a\widetilde{R}_t}{\widetilde{D}/\widetilde{H}} \tag{2.7}$$

is the Damköhler number, which is the ratio of reaction "velocity" to diffusion"velocity". It is seen in Table 2.1 that $\mathrm{Da_w} \gg 1$, which implies that reaction velocity is much faster than diffusion velocity. This is a direct consequence of the fact that there are multiple time and length scales associated with the experiment: ligand molecules must diffuse a distance on the order of millimeters to arrive at the reacting-surface, and the speed at which this happens is far slower than the reaction velocity.

Using the fact that $\mathrm{Da_w} \gg 1$ reduces (2.6) to

$$\frac{\partial B}{\partial t} = 0, \tag{2.8}$$

which implies that to leading-order $B(x,t)$ is in steady-state. Substituting (2.8) into (2.5) gives

$$C(\bar{x},0,t) = \frac{KB}{1-B}, \tag{2.9}$$

which implies that reaction happens so quickly that the unbound ligand concentration must adjust to the proper concentration at the surface. This reflects the diffusion-limited nature of the kinetics system under consideration: ligand molecules slowly diffuse through the well, and are very quickly incorporated into the surface. To study reaction dynamics we must examine diffusion of ligand molecules near the biochemical gate into the surface. To this end, we introduce the boundary layer coordinates

$$x = \frac{\bar{x}-1/2}{l_s}, \qquad y = \frac{\varepsilon}{l_s}\bar{y}. \tag{2.10}$$

In (2.10)

$$l_s = \frac{\widetilde{l}_\mathrm{s}}{\widetilde{L}} \tag{2.11}$$

is the ratio of biochemical gate length $\widetilde{l}_\mathrm{s}$ to the well length $\widetilde{L}$, and is very small. Introducing these scalings into (2.1a)–(2.1c) and (2.6) transform these equations into

$$\frac{\partial C}{\partial t} = D\left(\frac{\partial^2 C}{\partial x^2} + \frac{\partial^2 C}{\partial y^2}\right), \tag{2.12a}$$

$$C(x,y,0) = 0, \tag{2.12b}$$

$$C(x,\varepsilon/l_\mathrm{s},t) = 1, \tag{2.12c}$$

$$\frac{\partial C}{\partial x}(-1/(2l_\mathrm{s}),y,t) = \frac{\partial C}{\partial x}(1/(2l_\mathrm{s}),y,t) = 0, \tag{2.12d}$$

$$\frac{\partial C}{\partial y}(\bar{x},0,t) = \mathrm{Da}\frac{\partial B}{\partial t}\chi_\mathrm{s}. \tag{2.12e}$$

Furthermore, the kinetics equation (2.5) becomes

$$\frac{\partial B}{\partial t} = (1-B)C(x,0,t) - KB, \tag{2.13a}$$

$$B(x,0) = 0. \tag{2.13b}$$

Observe that transitioning to boundary layer coordinates has had the effect of rescaling D_w and Da_w. The parameter

$$D = \frac{\widetilde{D}}{\widetilde{l}_\mathrm{s}^2\widetilde{k}_\mathrm{a}\widetilde{C}_\mathrm{u}} = \frac{\widetilde{D}/\widetilde{l}_\mathrm{s}^2}{\widetilde{k}_\mathrm{a}\widetilde{C}_\mathrm{u}} \tag{2.14}$$

is the dimensionless diffusion coefficient on this length scale, and is the ratio of the diffusive time scale over a region of size $\widetilde{l}_\mathrm{s}^2$ to the forward reaction rate. From Table 2.1 it is seen that $D \gg 1$, which implies that diffusion over micrometer length scales is much faster than the forward reaction rate. This is intuitive since we are considering picomolar to femtomolar ligand concentrations. Furthermore

$$\mathrm{Da} = \frac{\widetilde{k}_\mathrm{a}\widetilde{R}_\mathrm{t}\widetilde{l}_\mathrm{s}}{\widetilde{D}} = \frac{\widetilde{k}_\mathrm{a}\widetilde{R}_\mathrm{t}}{\widetilde{D}/\widetilde{l}_\mathrm{s}} \tag{2.15}$$

is the Damköhler number on these length scales. Since Da is an $O(1)$ to $O(10)$ parameter, on these length scales reaction velocity is the same as or only slightly faster than the diffusion velocity. Equation (2.12e) then implies that reaction now balances with diffusion *near the surface* into receptors on the biochemical gate.

2.2 Integrodifferential Equation Reduction

Since $D \gg 1$, we neglect the left hand side of (2.12a) which reduces this equation to

$$\nabla^2 C = 0. \tag{2.16}$$

Physically, equation (2.16) implies that near the surface C is in a quasi-steady-state and change in the unbound concentration is driven by the surface-reaction (2.12e). Furthermore, since $l_s \ll 1$ we do not concern ourselves with satisfying the no-flux conditions (2.12d) and take our domain to be the infinite strip $\mathbb{R} \times [0, \varepsilon/l_s]$. This idealization is physically motivated and justified by the fact that the biochemical gate occupies a very narrow portion of the well surface, so the walls of the well will not appreciably affect ligand binding.

To solve the resulting set of PDEs we search for solutions of the form

$$C(x,y,t) = 1 + C_b(x,y,t), \tag{2.17}$$

where C_b satisfies

$$\nabla^2 C_b = 0, \tag{2.18a}$$
$$C_b(x, \varepsilon/l_s, t) = 0, \tag{2.18b}$$
$$\frac{\partial C_b}{\partial y}(x,0,t) = \mathrm{Da}\frac{\partial B}{\partial t}\chi_s, \tag{2.18c}$$

for $(x,y) \in \mathbb{R} \times [0, \varepsilon/l_s]$. To solve (2.18) we introduce a Fourier transform in x, defining the Fourier transform as

$$(\mathscr{F}u)(\omega) := \hat{u}(\omega) = \int_{-\infty}^{\infty} u(x) \mathrm{e}^{i\omega x}\, \mathrm{d}x, \tag{2.19a}$$

so that the inverse Fourier Transform is given by

$$(\mathscr{F}^{-1}\hat{u})(x) = u(x) = \frac{1}{2\pi}\int_{-\infty}^{\infty} \hat{u}(\omega) \mathrm{e}^{-i\omega x}\, \mathrm{d}x. \tag{2.19b}$$

Applying a Fourier transform to (2.18) and solving the resulting equation in frequency domain gives

$$\widehat{C}_b(\omega,y,t) = -\frac{\mathrm{Da}\ \sinh((\varepsilon l_s^{-1} - y)\omega)}{\omega \cosh(\varepsilon l_s^{-1}\omega)}\ \frac{\partial \widehat{B}}{\partial t}(\omega,t) \star \left(\frac{\sin(\omega/2)}{\omega/2}\right), \tag{2.20}$$

where the convolution product has been defined so that

$$\frac{\partial \widehat{B}}{\partial t}(\omega,t) \star \left(\frac{\sin(\omega/2)}{\omega/2}\right) = \int_{-\infty}^{\infty} \frac{\partial \widehat{B}}{\partial t}(\omega - \nu, t)\frac{\sin(\nu/2)}{\nu/2}\, \mathrm{d}\nu. \tag{2.21}$$

Now observe that in order to study the dynamics of interest, *i.e.* reaction, we need a closed-form for $C(x,y,t)$ only on the surface at $y = 0$. Thus it is sufficient to invert

$$\widehat{C}_b(\omega,0,t) = -\frac{\mathrm{Da}\ \tanh((\varepsilon l_s^{-1})\omega)}{\omega}\ \frac{\partial \widehat{B}}{\partial t}(\omega,t) \star \left(\frac{\sin(\omega/2)}{\omega/2}\right). \tag{2.22}$$

To this end we seek to apply the convolution theorem, and note that by duality

$$\mathscr{F}^{-1}\left(\frac{\partial \widehat{B}}{\partial t}(\omega,t) \star \left(\frac{\sin(\omega/2)}{\omega/2}\right)\right) = \frac{\partial B}{\partial t}(x,t)\chi_s(x). \tag{2.23}$$

Inverting (2.22) is then a matter of finding the inverse Fourier transform of

$$\widehat{f}(\omega) = \frac{\tanh(a\omega)}{\omega}, \quad a = \varepsilon l_{\mathrm{s}}^{-1}, \tag{2.24}$$

which requires computing

$$\mathscr{F}^{-1}(\widehat{f}(\omega)) = f(x) = \frac{1}{2\pi}\int_{-\infty}^{\infty} \frac{\tanh(a\omega)}{\omega} \mathrm{e}^{-i\omega x}\, \mathrm{d}\omega. \tag{2.25}$$

Observe that when $x = 0$ the integrand

$$\frac{\tanh(a\omega)}{\omega} = \frac{\mathrm{e}^{a\omega} - \mathrm{e}^{-a\omega}}{\omega(\mathrm{e}^{a\omega} + \mathrm{e}^{-a\omega})} \tag{2.26}$$

decays at a rate of $1/\omega$ as $\omega \to \pm\infty$. Thus (2.25) is not integrable when $x = 0$, and the inverse transform of $\hat{f}$ is singular at the origin. Evaluating the integral in (2.25) may then be broken up into two cases: when $x > 0$ and when $x < 0$. We first consider the latter by extending the integral into the complex plane in the manner depicted in Figure 2.1. To fix notation we let $C^{(n)} = \sum C_j^{(n)}$.

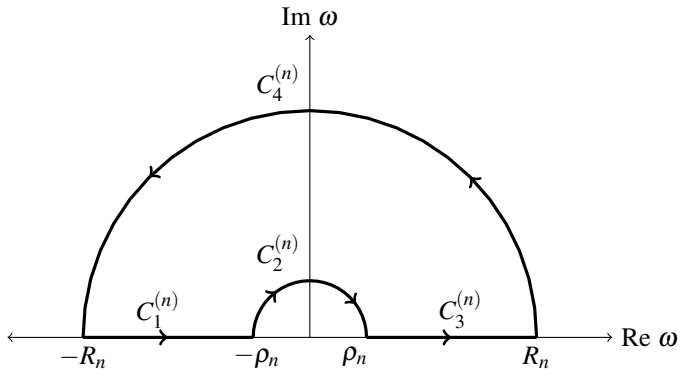

Figure 2.1: The contour used to calculate (2.25) when $x < 0$.

Since the hyperbolic tangent function has a countably infinite number of singularities along the imaginary axis, care must be taken to ensure that the path of integration does not intersect one of them. The singularities will occur when $\omega = 0$ or

$$\mathrm{e}^{\alpha\omega} + \mathrm{e}^{-\alpha\omega} = 0. \tag{2.27}$$

Note the contour depicted in Figure 2.1 does not pass through the singularity at the origin; in fact, since

$$\lim_{\omega\to 0} \tanh(a\omega) = 0 \tag{2.28}$$

this singularity would not have contributed to (3.5) if we had placed the semi-circle of radius ρ_n in the lower half-plane. Equation (2.27) then implies there are singularites at

$$\omega = \frac{\pi i(2n+1)}{2a}, \tag{2.29}$$

for each $n \in \mathbb{Z}$. Then taking the radii of our semi-circles to be

$$\rho_n = \pi/((n+2)a), \tag{2.30a}$$
$$R_n = \pi n/a, \tag{2.30b}$$

the path of integration will never intersect one of the singularities, and Cauchy's Residue Theorem may be applied:

$$\oint_{C^{(n)}} \frac{\tanh(a\omega)}{\omega} \mathrm{e}^{-i\omega x}\, \mathrm{d}\omega = 2\pi i \sum_{k=0}^{n-1} I(C^{(n)}, a_k)\, \mathrm{Res}\left(\frac{\tanh(a\omega)}{\omega}\mathrm{e}^{-i\omega x}; \alpha_n\right). \tag{2.31a}$$

In (2.31a) the singularities and their residues have been denoted

$$\alpha_k = \pi i(2k+1)/(2a), \tag{2.31b}$$
$$\mathrm{Res}\left(\frac{\tanh(a\omega)}{\omega}\mathrm{e}^{-i\omega x}; \alpha_k\right), \tag{2.31c}$$

and the winding number or index of $C^{(n)}$ with respect to a_k has been denoted by as

$$I(C^{(n)}, a_k). \tag{2.31d}$$

Since one may calculate the residues of the integrand in (2.25) to be

$$\mathrm{Res}\left(\frac{\tanh(a\omega)}{\omega}\mathrm{e}^{-i\omega x}; \alpha_k\right) = -\frac{2i\mathrm{e}^{(2k+1)\pi x/(2a)}}{\pi(2k+1)}, \tag{2.32}$$

Cauchy's Residue Theorem (2.31a) implies

$$\oint_{C^{(n)}} \frac{\tanh(a\omega)}{\omega} \mathrm{e}^{-i\omega x}\, \mathrm{d}\omega = 4\sum_{k=0}^{n-1} \frac{\mathrm{e}^{(2k+1)\pi x/(2a)}}{(2k+1)}, \tag{2.33}$$

and letting n approach infinity gives

$$\lim_{n\to\infty} \oint_{C^{(n)}} \frac{\tanh(a\omega)}{\omega} \mathrm{e}^{-i\omega x}\, \mathrm{d}\omega = 4\sum_{k=0}^{\infty} \frac{\mathrm{e}^{(2k+1)\pi x/(2a)}}{(2k+1)}. \tag{2.34}$$

On the other hand

$$\lim_{n\to\infty} \oint_{C^{(n)}} \frac{\tanh(a\omega)}{\omega}\, \mathrm{e}^{-i\omega x}\, \mathrm{d}\omega = \lim_{n\to\infty} \sum_{j=1}^{4} \oint_{C_j^{(n)}} \frac{\tanh(a\omega)}{\omega}\, \mathrm{e}^{-i\omega x}\, \mathrm{d}\omega. \tag{2.35}$$

As we shall show the second and fourth terms in the above sum vanish, leaving only contributions from the contours $C_1^{(n)}$ and $C_3^{(n)}$ which traverse the real line. First consider the second term; *i.e.*, the portion of the integral which traverses the contour $C_2^{(n)}$. Parameterizing $C_2^{(n)}$ by $\omega = \rho_n \mathrm{e}^{i\theta}$, for $\theta \in [\pi, 0]$, implies

$$\lim_{n\to\infty} \oint_{C_2^{(n)}} \frac{\tanh(a\omega)}{\omega} \mathrm{e}^{-i\omega x}\, \mathrm{d}\omega = \lim_{n\to\infty} i\int_{\pi}^{0} \tanh(a\rho_n \mathrm{e}^{i\theta}) \mathrm{e}^{\rho_n(-i\cos(\theta)+\sin(\theta))x}\, \mathrm{d}\theta, \tag{2.36}$$

and formally exchanging the limiting operations yields

$$i\int_{\pi}^{0}\lim_{n\to\infty}\tanh(a\rho_n e^{i\theta})e^{\rho_n(-i\cos(\theta)+\sin(\theta))x}\,d\theta=0 \tag{2.37}$$

since $\lim_{n\to\infty}\tanh(a\rho_n e^{i\theta})=0$. Thus, the contribution of (2.36) to (2.35) vanishes as $n\to\infty$. In a similar manner $C_4^{(n)}$ may be parameterized as $\omega=R_n e^{i\theta}$, for $\theta\in[\pi,0]$, to yield

$$\lim_{n\to\infty}\oint_{C_4^{(n)}}\frac{\tanh(a\omega)}{\omega}e^{-i\omega x}\,d\omega=\lim_{n\to\infty}i\int_0^{\pi}\tanh(aR_n e^{i\theta})e^{R_n(-i\cos(\theta)+\sin(\theta))x}\,d\theta. \tag{2.38}$$

Then formally exchanging the limiting operations gives

$$i\int_0^{\pi}\lim_{n\to\infty}\tanh(aR_n e^{i\theta})e^{R_n(-i\cos(\theta)+\sin(\theta))x}\,d\theta=0, \tag{2.39}$$

which follows since $x<0$, $\sin(\theta)>0$ almost everywhere on $[0,\pi]$, and the fact that $\tanh(aR_n e^{i\theta})$ remains bounded as $n\to\infty$.

Then since

$$\lim_{n\to\infty}\oint_{C_1^{(n)}}\frac{\tanh(a\omega)}{\omega}e^{-i\omega x}\,d\omega=\int_{-\infty}^{0}\frac{\tanh(a\omega)}{\omega}e^{-i\omega x}\,d\omega, \tag{2.40}$$

and

$$\lim_{n\to\infty}\oint_{C_3^{(n)}}\frac{\tanh(a\omega)}{\omega}e^{-i\omega x}\,d\omega=\int_{0}^{\infty}\frac{\tanh(a\omega)}{\omega}e^{-i\omega x}\,d\omega, \tag{2.41}$$

equation (2.35) implies

$$\lim_{n\to\infty}\oint_{C^{(n)}}\frac{\tanh(a\omega)}{\omega}e^{-i\omega x}\,d\omega=\int_{-\infty}^{\infty}\frac{\tanh(a\omega)}{\omega}e^{-i\omega x}\,d\omega. \tag{2.42}$$

Moreover, (2.34) together with (2.42) implies

$$\int_{-\infty}^{\infty}\frac{\tanh(a\omega)}{\omega}e^{-i\omega x}\,d\omega=4\sum_{n=0}^{\infty}\frac{e^{(2k+1)\pi x/(2a)}}{(2k+1)}. \tag{2.43}$$

However, the Maclaurin expansion for the inverse hyperbolic tangent function is

$$\tanh^{-1}(x)=\sum_{k=0}^{\infty}\frac{x^{2k+1}}{2k+1}. \tag{2.44}$$

Hence when $x<0$ the inverse Fourier transform of (2.24) is given by

$$f(x)=\frac{2}{\pi}\tanh^{-1}(e^{\pi l_s x/(2\varepsilon)}). \tag{2.45}$$

It remains to find the inverse Fourier transform of (2.24) when $x>0$; this is done in analogous manner by extending (2.47) into the complex plane in the manner depicted in (2.2). Doing so and using arguments similar to those for the case when $x<0$ leads

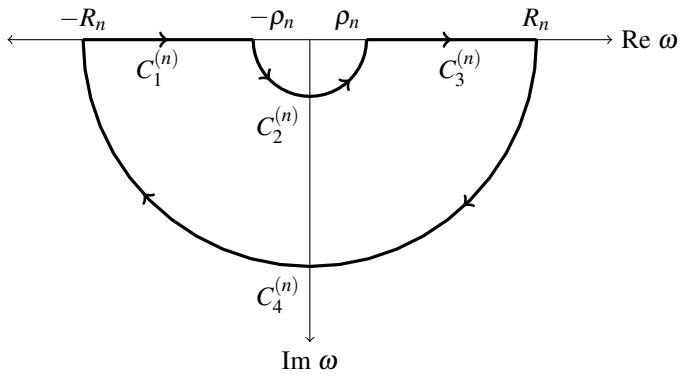

Figure 2.2: The contour used to calculate (2.25) when $x < 0$.

to the conclusion that

$$f(x) = \frac{2}{\pi}\tanh^{-1}(\mathrm{e}^{-\pi l_s x/(2\varepsilon)}) \tag{2.46}$$

when $x > 0$.

In summary: the inverse transform of (2.24) is singular at the origin, (2.45) when $x < 0$, and (2.46) when $x > 0$. Putting these three observations together leads to the conclusion that the inverse Fourier transform of (2.24) is

$$f(x) = \tanh^{-1}(\mathrm{e}^{-\pi l_s|x|/(2\varepsilon)}). \tag{2.47}$$

Since the inverse Fourier transform of (2.24) is (2.47), the convolution theorem may be applied to invert (2.20). Doing so gives

$$C_\mathrm{b}(x,0,t) = -\frac{2\,\mathrm{Da}}{\pi}\int_{-\infty}^{\infty}\tanh^{-1}(\mathrm{e}^{-\pi l_s|x-\nu|/(2\varepsilon)})\frac{\partial B}{\partial t}(\nu,t)\chi_\mathrm{s}(\nu)\,\mathrm{d}\nu \tag{2.48}$$

or

$$C_\mathrm{b}(x,0,t) = -\frac{2\,\mathrm{Da}}{\pi}\int_{-1/2}^{1/2}\tanh^{-1}(\mathrm{e}^{-\pi l_s|x-\nu|/(2\varepsilon)})\frac{\partial B}{\partial t}(\nu,t)\,\mathrm{d}\nu. \tag{2.49}$$

Having solved for $C_\mathrm{b}(x,0,t)$, from (2.17) we conclude

$$C(x,0,t) = 1 + C_\mathrm{b}(x,0,t) = 1 - \frac{2\,\mathrm{Da}}{\pi}\int_{-1/2}^{1/2}\tanh^{-1}(\mathrm{e}^{-\pi l_s|x-\nu|/(2\varepsilon)})\frac{\partial B}{\partial t}(\nu,t)\,\mathrm{d}\nu.$$

Hence bound ligand evolution is governed by the IDE:

$$\frac{\partial B}{\partial t} = (1-B)\left(1 - \frac{2\,\mathrm{Da}}{\pi}\int_{-1/2}^{1/2}\tanh^{-1}(\mathrm{e}^{-\pi l_s|x-\nu|/(2\varepsilon)})\frac{\partial B}{\partial t}(\nu,t)\,\mathrm{d}\nu\right) - KB, \tag{2.50a}$$

$$B(x,0) = 0. \tag{2.50b}$$

3 Numerical Method

3.1 Method of Lines Approximation

The IDE (2.50) is nonlinear and unwieldy, so we now search for a numerical approximation to its solution. First we choose N equally-spaced discretization nodes x_i and partition $[-1/2, 1/2]$ into N distinct subintervals of length $\Delta x = 1/N$:

$$\left[-\frac{1}{2}, \frac{1}{2}\right] = \bigcup_{i=1}^{N} \left[x_i - \frac{\Delta x}{2}, x_i + \frac{\Delta x}{2}\right], \tag{3.1}$$

where $-1/2 = x_1 - \Delta x/2$ and $1/2 = x_N + \Delta x/2$. Next we seek to apply the method of lines by proposing an approximation of the form:

$$B(x,t) \approx \sum_{i=1}^{n} h_i(t)\phi_i(x). \tag{3.2}$$

The functions $h_i(t)$ are to be deterimine and subject to the initial condition $h_i(0) = 0$, while the functions $\phi_i(x)$ are locally defined hat functions given as

$$\phi_i(x) = \begin{cases} \dfrac{2}{\Delta x}[x - (x_i - \Delta x/2)] & \text{if } x \in [x_i - \Delta x/2, x_i), \\ \dfrac{2}{\Delta x}[(x_i + \Delta x/2) - x] & \text{if } x \in [x_i, x_i + \Delta x/2], \\ 0 & \text{else.} \end{cases} \tag{3.3}$$

Substituting (3.2) into (2.50a) and evaluating each side of the resulting equation at $x = x_j$ yields

$$h_j'(t) = (1 - h_j(t))\left(1 - \sum_{i=1}^{N} \frac{2\,\mathrm{Da}\, h_i'(t)}{\pi} \int_{-1/2}^{1/2} \tanh^{-1}(\mathrm{e}^{-|x_j - \nu|\pi l_s/(2\varepsilon)})\phi_i(\nu)\,\mathrm{d}\nu\right) - Kh_j(t), \tag{3.4}$$

for $j = 1, \ldots, N$. The solution of this nonlinear set of ODEs determines the time-dependent functions $h_j(t)$, however solving this system requires computing

$$\int_{-1/2}^{1/2} \tanh^{-1}(\mathrm{e}^{-|x_j - \nu|\pi l_s/(2\varepsilon)})\phi_i(\nu)\,\mathrm{d}\nu. \tag{3.5}$$

Since $\tanh^{-1}(\mathrm{e}^{-|x_j - \nu|\pi l_s/(2\varepsilon)})$ exhibits logarithmic singularity at $\nu = x_j$, computing (3.5) using a quadrature rule requires great care, although (3.5) can be computed exactly. This is done by decomposing the basis functions (3.3) into their left and right parts:

$$\phi_{i,l}(x) = \begin{cases} \dfrac{2}{\Delta x}[x - (x_i - \Delta x/2)] & \text{if } x \in [x_i - \Delta x/2, x_i), \\ 0 & \text{else,} \end{cases} \tag{3.6}$$

and

$$\phi_{i,r}(x) = \begin{cases} \dfrac{2}{\Delta x}[(x+x_i) - \Delta x/2] & \text{if } x \in [x_i, x_i + \Delta x/2], \\ 0 & \text{else.} \end{cases} \tag{3.7}$$

Having decomposed the basis functions into their left and right parts (3.5) can be written as

$$\begin{aligned} \int_{-1/2}^{1/2} \tanh^{-1}(\mathrm{e}^{-|x_j-\nu|\pi l_\mathrm{s}/(2\varepsilon)})\phi_i(\nu)\,\mathrm{d}\nu = &\int_{-1/2}^{1/2} \tanh^{-1}(\mathrm{e}^{-|x_j-\nu|\pi l_\mathrm{s}/(2\varepsilon)})\phi_{i,l}(\nu)\,\mathrm{d}\nu \\ &+ \int_{-1/2}^{1/2} \tanh^{-1}(\mathrm{e}^{-|x_j-\nu|\pi l_\mathrm{s}/(2\varepsilon)})\phi_{i,r}(\nu)\,\mathrm{d}\nu. \end{aligned} \tag{3.8}$$

Since the two terms on the right hand side are related through a change of variables, it is sufficient to calculate

$$\int_{-1/2}^{1/2} \tanh^{-1}(\mathrm{e}^{-|x_j-\nu|\pi l_\mathrm{s}/(2\varepsilon)})\phi_{i,l}(\nu)\,\mathrm{d}\nu. \tag{3.9}$$

After changing variables, one may use the definition of $\tanh^{-1}(\cdot)$ and expand the integrand in terms of its Mclaurin series to find that it is a telescoping sum:

$$\int_{-1/2}^{1/2} \tanh^{-1}(\mathrm{e}^{-|x_j-\nu|\pi l_\mathrm{s}/(2\varepsilon)})\phi_{i,l}(\nu)\,\mathrm{d}\nu = \sum_{n=0}^{\infty} \frac{2}{\Delta x} \int_0^{\Delta x/2} \frac{\mathrm{e}^{-|w-x_j+x_i-\Delta x/2|(2n+1)/(2\varepsilon)}}{2n+1} w\,\mathrm{d}w. \tag{3.10}$$

In writing (3.10) we have formally exchanged the limit operations. Observe that the absolute value prevents one from integrating by parts directly; however, by using the fact that the discretization nodes are equally spaced one can show the computation may be partitioned in two distinct cases: when $x_j \geq x_i$ and $x_j < x_i$. Since the computation is analogous in each case we concern ourselves only with the former. Thus taking $x_j \geq x_i$ and integrating the right hand side of (3.10) by parts shows that (3.9) is equal to

$$\begin{aligned} \sum_{n=0}^{\infty} \left(\frac{2}{\Delta x}\right) \Bigg(&\frac{\Delta x \varepsilon\, \mathrm{e}^{-(x_j-x_i)(2n+1)\pi l_\mathrm{s}/(2\varepsilon)}}{(2n+1)^2 \pi l_\mathrm{s}} - \frac{4\varepsilon^2\, \mathrm{e}^{-(x_j-x_i)(2n+1)\pi l_\mathrm{s}/(2\varepsilon)}}{(2n+1)^3 \pi^2 l_\mathrm{s}^2} \\ &+ \frac{4\varepsilon^2\, \mathrm{e}^{-[\Delta x/2+(x_j-x_i)](2n+1)\pi l_\mathrm{s}/(2\varepsilon)}}{(2n+1)^3 \pi^2 l_\mathrm{s}^2} \Bigg). \end{aligned} \tag{3.11}$$

To sum the series (3.11), we observe that one can use the definition of the polylogarithm of order s

$$\mathrm{Li}_\mathrm{s}(z) = \sum_{k=1}^{\infty} \frac{z^k}{k^s} \tag{3.12}$$

to show

$$\sum_{n=0}^{\infty} \frac{z^{2n+1}}{(2n+1)^s} = \mathrm{Li}_\mathrm{s}(z) - \frac{1}{2^\mathrm{s}} \mathrm{Li}_s(z^2). \tag{3.13}$$

Hence when $x_j \geq x_i$

$$\begin{aligned}
&\int_{-1/2}^{1/2} \tanh^{-1}(\mathrm{e}^{-|x_j-\nu|\pi l_\mathrm{s}/(2\varepsilon)})\phi_{i,l}(\nu)\,\mathrm{d}\nu \\
&\quad = \left(\frac{2}{\Delta x}\right)\left[\frac{\Delta x\varepsilon}{\pi l_\mathrm{s}}\left(\mathrm{Li}_2(\mathrm{e}^{-(x_j-x_i)\pi l_\mathrm{s}/(2\varepsilon)}) - \mathrm{Li}_2(\mathrm{e}^{-(x_j-x_i)\pi l_\mathrm{s}/(\varepsilon)})/4\right)\right. \\
&\qquad - \frac{4\varepsilon^2}{\pi^2 l_\mathrm{s}^2}\left(\mathrm{Li}_3(\mathrm{e}^{-(x_j-x_i)\pi l_\mathrm{s}/(2\varepsilon)}) - \mathrm{Li}_3(\mathrm{e}^{-(x_j-x_i)\pi l_\mathrm{s}/(\varepsilon)})/8\right) \\
&\qquad \left. + \frac{4\varepsilon^2}{\pi^2 l_\mathrm{s}^2}\left(\mathrm{Li}_3(\mathrm{e}^{-[\Delta x/2+(x_j-x_i)]\pi l_\mathrm{s}/(2\varepsilon)}) - \mathrm{Li}_3(\mathrm{e}^{-[\Delta x/2+(x_j-x_i)]\pi l_\mathrm{s}/(\varepsilon)})/8\right)\right].
\end{aligned} \tag{3.14}$$

The form of (3.14) when $x_j < x_i$ is very similar. With the exact value of (3.8), the nonlinear set of ODEs (3.4) can be solved using one's favorite linear multistage or multistep formula.

3.2 Convergence

Convergence of the numerical method outlined in the previous Subsection was measured by first computing a reference solution $B_\mathrm{ref}(x,t)$ on a mesh with $N = 3^7 = 2187$ spatial discretization nodes; this was done by integrating (3.4) from $t = 0$ to $t = 150$ using an adaptive linear multistage formula. Then solutions $B_i(x,t)$ were computed on meshes with $N = 3^i$ nodes and convergence was measured by calculating

$$|| \, ||B_\mathrm{ref}(x,t) - B_i(x,t)||_{2,\,x}||_{\infty,\,t} \tag{3.15}$$

for $i = 1, \ldots, 6$. In (3.15) $||\cdot||_{2,\,x}$ denotes l_2 norm in x and $||\cdot||_{\infty,\,t}$ denotes the infinity norm in t. A logarithmic plot of these values is depicted in Figure 3.1. Despite the logarithmic singularity in (2.50a), the evidence in Figure 3.1 strongly suggests that our method of lines approximation to (2.50) achieves first-order convergence. Although it is of interest to derive analytic error estimates for our approximation, the nonlinearity in (2.50a) seems to render any such estimates beyond reach.

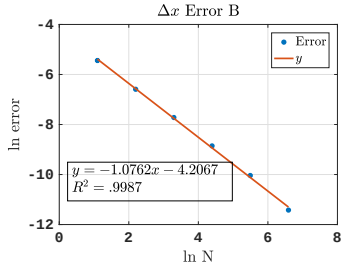

Figure 3.1: The values of (3.15) for $i = 1, \ldots, 6$ depicted together with the line $y = -1.0762x - 4.2067$, which was fit to the values of (3.15) with an R^2 coefficient of $R^2 = .9987$. These simulations were computed using the parameter values $\mathrm{Da} = 66.42$, $K = 1$, $l_\mathrm{s} = 10^{-3}$, and $\varepsilon = 1$.

4 Results and Discussion

Results of our numerical simulations are depicted in Figure 4.1. Upon inspection one immediately notices the presence of a depletion region in the middle of the sensor for small t. As time progresses the rate of bound ligand production near the boundary decreases and the depletion region narrows. The bound ligand concentration continues to become more spatially uniform until a uniform chemical equilibrium is achieved in which there is a balance between association and dissociation.

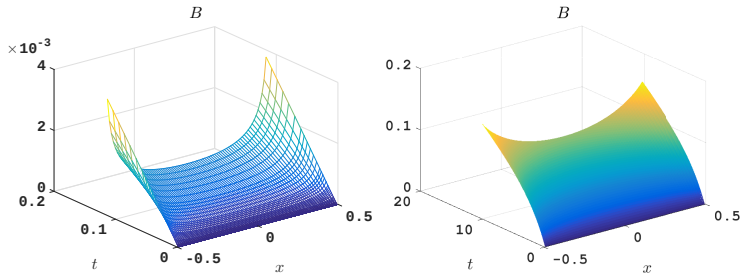

(a) Evolution of $B(x,t)$ for $t \in [0,.1]$

(b) Evolution of $B(x,t)$ for $t \in [0,10]$.

(c) Evolution of $B(x,t)$ for $t \in [0,50]$.

(d) Evolution of $B(x,t)$ for $t \in [0,150]$.

Figure 4.1: Numerical solution to (2.50) during different time intervals using the parameter values $\mathrm{Da} = 66.42$, $K = 1$, $l_s = 10^{-3}$, and $\varepsilon = 2/5$.

Mathematically, the depletion region results from the singular convolution kernal

$$\tanh^{-1}(e^{-|(x-\nu)|\pi l_s/(2\varepsilon)}) \tag{4.1}$$

and the finite limits of integration. In Figure 4.2 we have depicted our convolution kernal centered at $x = 0$, and $x = -1/2$. When the convolution kernal is centered at $x = 0$ it acts as a two-sided influence function. The singularity at $x = 0$ reflects the high likelihood that a ligand molecule directly above the origin will diffuse to the surface and bind with an available receptor site there; however, in the unstirred layer ligand molecules diffusing into the surface bind with neighboring receptor sites. Figure 4.2 reveals the likelihood of binding with a neighboring receptor site decays with the distance away from the source, although it is never zero since $\tanh^{-1}(e^{-|x-\nu|\pi l_s}/(2\varepsilon))$

is supported almost everywhere on the real line, and in particular, almost everywhere on $[-1/2, 1/2]$.

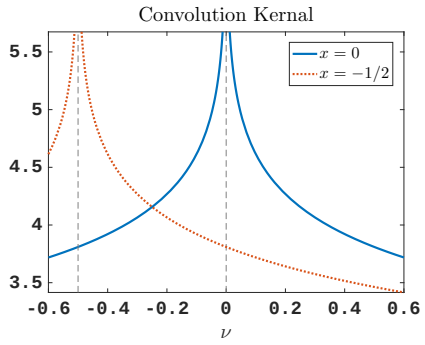

Figure 4.2: The convolution kernal $\tanh^{-1}(e^{-|x-\nu|\pi l_s/(2\varepsilon)})$ centered at $x = 0$ (solid line), and at $x = -1/2$ (dotted line). Here $l_s = 10^{-3}$, and $\varepsilon = 2/5$.

Conversely, when the kernal is centered at $x = -1/2$ Figure 4.2 shows that it acts as a one-sided influence function. The finite limits of integration in (2.50a) imply that the convolution kernal influences the bound ligand concentration the most at $x = -1/2$, and has a monotonically decreasing influence as one progresses from $x = -1/2$ to $x = 1/2$. Thus we see the finite limits of integration encode the reflective boundary conditions. To the right of $x = -1/2$, ligand molecules spread out and diffuse into the surface; to the left, ligand molecules are reflected.

Furthermore, from (2.50a) we see that the size of the depletion region is directly related to Da–larger values of Da correspond to more pronounced depletion regions at a fixed time t. From (2.15) it is seen larger values of Da correspond to larger ratios of reaction velocity to diffusion velocity. When the reaction velocity $\widetilde{k}_a\widetilde{R}_t$ is much faster than diffusion velocity $\widetilde{D}/\widetilde{l}_s$, the additional ligand flux from the one-sided decay near the boundaries results in the reaction proceeding faster in the enrichment regions. Figure 4.3 shows the bound ligand evolution after $t = 10$ seconds when $\mathrm{Da} = 5.5352$, and when $\mathrm{Da} = 33.2110$. Clearly, the depletion region is more significant when $\mathrm{Da} = 33.2110$.

Moreover, Figure 4.3 shows that Da affects how fast reaction proceeds. Indeed, from Figure 4.3 it is seen that reaction proceeds at a slower rate when Da is larger. This agrees with our above discussion: larger values of Da correspond to a wider depletion region, and the rate of reaction depends upon the amount of unbound ligand at the surface $C(x,0,t)$.

Although Da is $O(1)$ or larger, it is illuminating to consider the limit in which $\mathrm{Da} \to 0$; *i.e.*, when (2.50a) reduces to a simple ODE. This is the classical well-stirred approximation, in which reaction kinetics completely decouple from diffusion into the surface. Physically, in this case, ligand molecules arrive at surface on a much faster time scale than reaction. We expect reaction to proceed more quickly in this regime, because the rate at which it occurs is limited by the intrinsic rate constants $\widetilde{k}_a$, $\widetilde{k}_d$ and the ligand concentration $\widetilde{C}_u$. Thus, this is the reaction-limited regime.

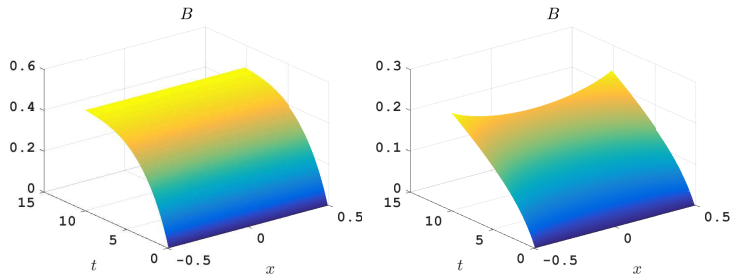

(a) The solution of (2.50) with Da = 5.5352.

(b) The solution of (2.50) with Da = 33.2110.

Figure 4.3: Numerical solution to (2.50) after $t = 10$ seconds for different values of Da. Notice the different scales on the z-axis. In each of these simulations the parameter values $K = 1$, $l_s = 10^{-3}$, and $\varepsilon = 2/5$ were used.

Conversely, when $\mathrm{Da} = O(1)$ or larger reaction and diffusion near the surface into the sensor occur on the same time scale. Thus, the fact that $\mathrm{Da} = O(1)$ or larger reflects the fast nature of our reaction, and the relatively slow nature of diffusion near the surface into the sensor. In this regime, the speed at which the reaction proceeds depends not only upon the rate constants $\widetilde{k}_a$, $\widetilde{k}_d$ and the ligand concentration $\widetilde{C}_u$, but also upon the speed at which ligand molecules diffuse into the surface. Since diffusion is a relatively slow process, we expect the reaction to proceed slower in this regime. This phenomenon is depicted Figure 4.3, where it is seen that increasing Da reduces the rate at which reaction proceeds.

5 Conclusions

The nanoscale electronics experiment under consideration has been modeled with a diffusion equation, coupled to an equation describing reaction on the sensor surface. By using the appropriate time and length scales the evolution of C may be described with the quasi-steady approximation. By solving this equation in frequency domain and inverting at $y = 0$ with Cauchy's Residue Theorem, we have obtained a formula for $C(x,0,t)$. This reduces the full PDE system to a single nonlinear IDE for B. Despite the presence of a nonlinear singular convolution kernal, this equation has been solved to first-order accuracy without resorting to quadrature techniques to evaluate (3.5). Results of our numerical simulations reveal the presence of a depletion region in the middle of the sensor. Mathematically, the depletion region results from the finite limits of integration and the convolution kernal. The finite limits of integration encode the reflective boundary conditions, and the convolution kernal captures the effect of diffusion into the surface. Moreover, the effect of diffusion into the surface is directly tied to Da–larger values of Da result in a more pronounced depletion region at a given time t.

In the future, we would like to investigate the dynamics of this system under experimental conditions. In particular, an sealed experiment with an initial drop of ligands. This corresponds to a no-flux boundary condition on the top, and a compactly supported Gaussian as our initial condition.

Acknowledgements

The first author would like to thank Enrique Zuazua for making possible a very stimulating visit at the University of Deusto during which many aspects of this work were thoroughly discussed.

References

[1] M. H. Abouzar, A. Poghossian, A. G. Cherstvy, A. M. Pedraza, S. Ingebrandt, and M. J. Schöning. Label-free electrical detection of DNA by means of field-effect nanoplate capacitors: experiments and modeling. *Physica Status Solidi (a)*, 209(5):925–934, 2012.

[2] S. Baumgartner, M. Vasicek, A. Bulyha, N. Tassotti, and C. Heitzinger. Analysis of field-effect biosensors using self-consistent 3D drift-diffusion and Monte-Carlo simulations. *Procedia Engineering*, 25:407–410, 2011.

[3] J. L. Gomez and O. Tigli. Modeling and simulation of zinc oxide nanowire field effect transistor biosensor. In *Nanotechnology Materials and Devices Conference*, pages 412–415. IEEE, 2011.

[4] C. Heitzinger, N. J. Mauser, and C. Ringhofer. Multiscale modeling of planar and nanowire field-effect biosensors. *SIAM Journal on Applied Mathematics*, 70(5):1634–1654, 2010.

[5] D. Landheer, G. Aers, W. R. McKinnon, M. J. Deen, and J. C. Ranuarez. Model for the field effect from layers of biological macromolecules on the gates of metal-oxide-semiconductor transistors. *Journal of Applied Physics*, 98(4):044701, 2005.

[6] P. R. Nair and M. A. Alam. Design considerations of silicon nanowire biosensors. *IEEE Transactions on Electron Devices*, 54(12):3400–3408, 2007.

[7] G. Tulzer, S. Baumgartner, E. Brunet, G. C. Mutinati, S. Steinhauer, A. Köck, P. E. Barbano, and C. Heitzinger. Kinetic parameter estimation and fluctuation analysis of CO at SnO_2 single nanowires. *Nanotechnology*, 24(31):315501, 2013.

[8] Y. Wang and G. Li. Performance investigation for a silicon nanowire fet biosensor using numerical simulation. In *Nanotechnology Materials and Devices Conference*, pages 81–86. IEEE, 2010.